Nano Energy 102 (2022) 107692

Contents lists available at ScienceDirect

Nano Energy

journal homepage: www.elsevier.com/locate/nanoen

Ice-assisted electron-beam lithography for halide perovskite optoelectronic nanodevices

Binbin Jin [a,b,c], Yu Hong [d], Ziqing Li [e], Ding Zhao [a,c,*], Yihan Lu [a,c], Guangnan Yao [a,c], Rui Zheng [a,c], Gang Bi [b], Qing Zhang [f], Xiaosheng Fang [e,**], Min Qiu [a,c,*]

[a] Key Laboratory of 3D Micro/Nano Fabrication and Characterization of Zhejiang Province, School of Engineering, Westlake University, 18 Shilongshan Road, Hangzhou 310024, Zhejiang Province, China
[b] School of Information & Electrical Engineering, Zhejiang University City College, 48 Huzhou Street, Hangzhou 310015, Zhejiang Province, China
[c] Institute of Advanced Technology, Westlake Institute for Advanced Study, 18 Shilongshan Road, Hangzhou 310024, Zhejiang Province, China
[d] Key Laboratory of Modern Optical Instrumentation, College of Optical Science and Engineering, Zhejiang University, Hangzhou 310027, China
[e] Institute of Optoelectronics, Department of Materials Science, Fudan University, Shanghai 200433, China
[f] School of Materials Science and Engineering, Peking University, Beijing 100871, China

ARTICLE INFO

Keywords:
Ice lithography
E-beam lithography
Perovskite photodetector
Solvent-free nanofabrication
In-situ imaging

ABSTRACT

Metal halide perovskites (MHPs) have received substantial attention due to their impressive optoelectronic properties. In particular, nanoscale perovskite structures, such as nanowires (NWs) and nanoplates (NPs) are ideal building blocks for optoelectronic devices. However, metal electrodes can be hardly patterned on these materials with conventional lithographic methods due to the solvent sensitivity of perovskite crystals and alignment issues. Here, we report a solvent-free method to fabricate metal electrodes on perovskite NPs, which starts with the vapor deposition of water ice as an electron resist and ends in the sublimation of the ice followed by a "blow-off" process. The good compatibility between MHPs and ice as well as the in-situ imaging and patterning process guarantees the fabrication with high precision and resolution. Using this technique, we create metal electrodes on single-crystal $MAPbBr_3$ NPs featuring a nanoscale gap of 296 nm and superior photodetection ability with responsivity of 653 A/W and detectivity of 3.08×10^{13} Jones. Our study helps the widely-used electron-beam lithography break down barriers in processing perovskite materials, and provides an excellent platform to fully exploit their potentials in optoelectronic devices.

1. Introduction

The development of optoelectronic nanodevices is inseparable from the exploration of new semiconductor materials and innovative processing techniques [1,2]. As one class of promising semiconductors, organic-inorganic hybrid halide perovskites ($MAPbX_3$, $MA{=}CH_3NH_3^+$, $X{=}Cl^-$, Br^-, I^-) are of particular interest due to their large light absorption coefficient, long carrier diffusion length and high carrier mobility [3-5]. These impressive properties make perovskites excellent semiconductors for solar cells, photodetector, LEDs and lasers. Besides, processing temperature of perovskite materials is quite low (less than 150 ℃), enabling them to integrate with plastic or polymer substrates for flexible devices. In contrast to conventional vacuum processing, all-solution based synthetic route enables the production of single-crystalline perovskites with excellent optoelectronic properties [6-9]. However, the solubility of perovskites is also somewhat of a double-edge sword. It is thus difficult to make electrodes on perovskites through solution-processing steps [10–12]. For instance, electron-beam lithography (EBL) is currently the most widespread and reliable manufacturing method for fabricating electrodes when nanoscale dimensions are needed [13,14]. The technique requires a standard process including spin-coating, electron-beam (e-beam) patterning, chemical development, metal deposition and lift-off. Unfortunately, abundant polar solvents such as anisole, methyl isobutyl ketone, isopropyl alcohol and acetone, which can readily degrade the perovskite crystals, are inevitably employed in the lithographic process.

Reducing exposure to solvents in nanofabrication is thus the first essential to build perovskite nanodevices. A simplistic approach to

* Corresponding authors at: School of Engineering, Westlake University, Hangzhou 310024, Zhejiang Province, China.
** Correspondence to: Department of Materials Science, Fudan University, Shanghai 200433, China.
E-mail addresses: zhaoding@westlake.edu.cn (D. Zhao), xshfang@fudan.edu.cn (X. Fang), qiu_lab@westlake.edu.cn (M. Qiu).

https://doi.org/10.1016/j.nanoen.2022.107692
Received 8 June 2022; Received in revised form 27 July 2022; Accepted 8 August 2022
Available online 10 August 2022

patterning on perovskites is utilizing area-selective deposition through a shadow mask or stencil where metals can be evaporated directly onto perovskites in a desired pattern [15-20]. Mechanical transfer of perovskites to prepatterned structures alternatively meets such an expectation. But both methods have limitations in positioning and alignment during nanofabrication. Recently, efforts have been made to optimize the standard EBL process for developing a perovskite-compatible lithography method with nanoscale precision. Orthogonal lithography by substituting high polar solvents (isopropyl alcohol and acetone) with the low polar (chlorobenzene: dissolving resist; hexane: resist development) successfully fabricated 2D perovskite photodetectors featuring excellent photoresponse [21]. A perovskite photodetector can also be obtained by employing a double layer of resists with different molecular weights [22]. Despite plenty of advancements, solvents are not avoided in these strategies, leading to complicated nanofabrication procedures with a high risk of damaging perovskite structures.

Here, we demonstrate that ice-assisted EBL (iEBL) [23,24], utilizing water ice as an electron resist, can easily fabricate nanoscale metal patterns onto perovskites. It is an utterly solvent-free procedure which starts with vapor deposition of water ice and ends in the sublimation of the ice followed by a "blow-off" process. Only water ice involved indicates no resist contamination in the whole procedure, which is a major concern in conventional lithography methods. Moreover, advantages of in-situ imaging and patterning in iEBL guarantee accurate positioning of fabricated nanostructures. After carefully investigating the compatibility between perovskites and water ice, we have fabricated a perovskite photodetector featuring nanoscale patterned electrodes and superior photodetection ability with responsivity of 653 A/W and detectivity of 3.08×10^{13} Jones. Our study provides a simple, efficient, and eco-friendly way for constructing nanostructures on perovskites. It can be well integrated with traditional semiconductor manufacturing processes, beneficial to fully exploit potentials of perovskites in

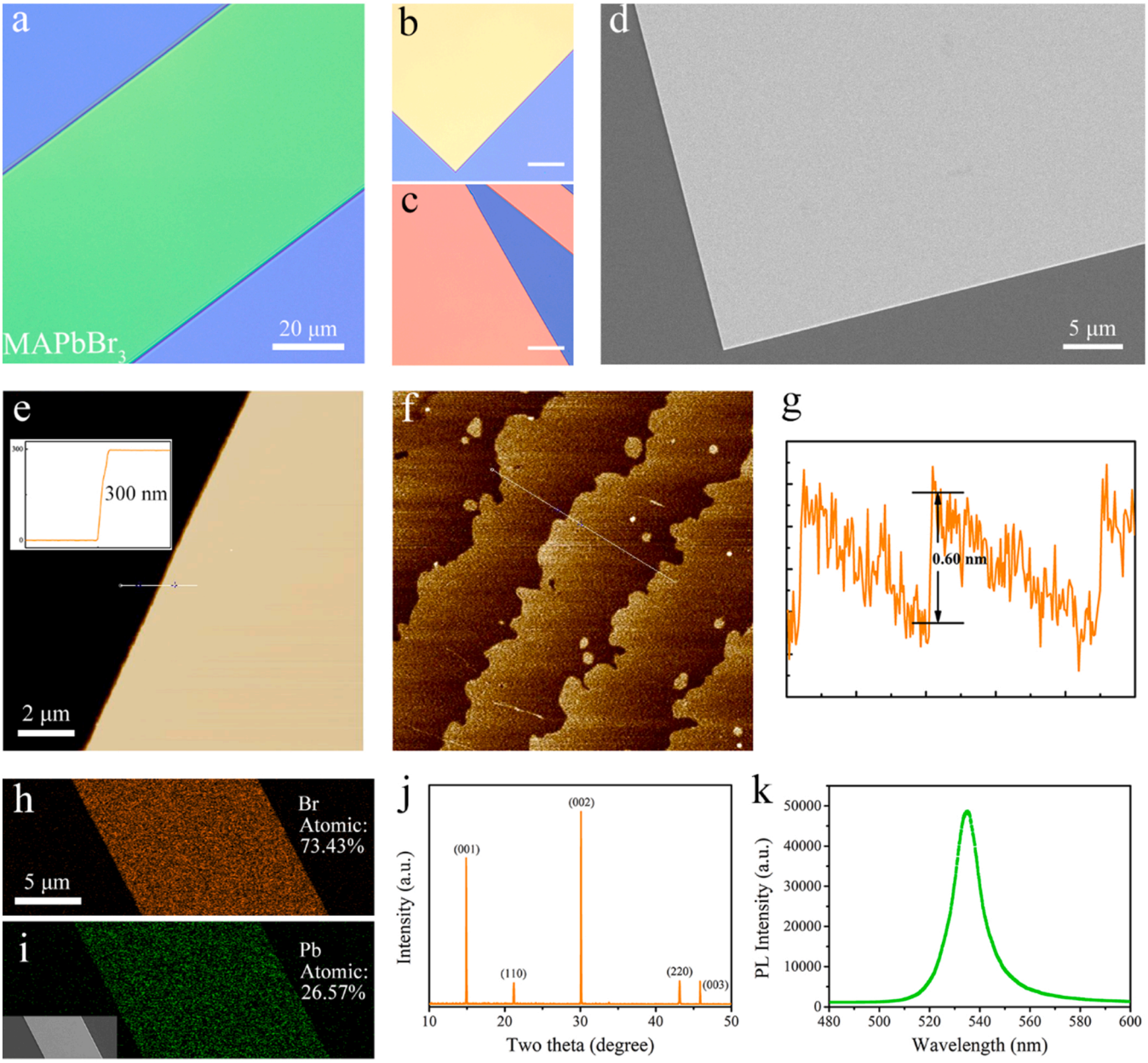

Fig. 1. Characterization of $MAPbBr_3$ NPs. (a-c) Optical images $MAPbBr_3$ NPs showing the thickness-dependent colors. (d) SEM image of $MAPbBr_3$ NP with thickness of 300 nm. (e) AFM images of $MAPbBr_3$ NP with thickness of 300 nm and (f and g) monolayer height profile. EDS mapping of (h) Br and (i) Pb elements. (j) XRD pattern of $MAPbBr_3$ NPs. (k) PL spectrum of $MAPbBr_3$ NPs.

optoelectronic devices.

2. Results and discussion

The space-confined growth method is used to obtain single-crystalline $MAPbBr_3$ NPs with controllable thickness down to a few hundred nanometers [25-29]. In this process, the confined space is constructed by a hydrophilic and a hydrophobic Si/SiO_2 substrates (Figs. S1 and S2). The thickness of $MAPbBr_3$ is well-defined by the pressure applied to the substrates. As illustrated in Fig. 1a-c, $MAPbBr_3$ NPs with various thickness in nanometer range exhibit characteristic colors due to the effect of thin film interference (Fig. S3). This simple and direct visual inspection helps us harvest a certain thickness film to meet diverse applications [30-32]. The scanning electron microscope (SEM) image discloses the smooth surface that is free of domain and grain boundaries (Fig. 1d). Atomic force microscopy (AFM) studies show that the green $MAPbBr_3$ NP exhibits a film thickness of ~300 nm (Fig. 1e) and a nearly atomically flat surface with a room-mean-square roughness of ~0.443 nm. Moreover, a monolayer of a cubic $MAPbBr_3$ unit cell with a height ~0.6 nm is also observed in Fig. 1f and g. The energy-dispersive X-ray spectroscopy (EDS) mapping image indicates the uniform distribution of Br and Pb elements with the composition ratio close to the theoretical value (Fig. 1h and i). X-ray diffraction (XRD) also confirms the high purity of $MAPbBr_3$ crystal in cubic phase (Fig. 1j). Fig. 1k shows the photoluminescence (PL) spectrum with a single emission peak at ~535 nm, consistent with the band-edge emission in $MAPbBr_3$. The obtained $MAPbBr_3$ NPs with smooth surface and high degree crystallinity is essential for ensuring an intimate contacting with the electrodes to enable the formation of ohmic contacts.

Generally, the presence of liquid water leads to the irreversible decomposition of $MAPbX_3$ to PbX_2 [33-35]. In contrast to liquid water, moisture in the form of ambient humidity is beneficial to heal the defect states of $MAPbBr_3$ through hydrogen bonding or partial solvation of methylammonium component [36,37]. In our experiment, we first verify whether single-crystalline $MAPbBr_3$ NP is compatible with ice deposition. Water vapor was sprayed on the surface of $MAPbBr_3$ NP to form a uniform film of amorphous ice at 130 K (see Supplementary Information for details) [23], and the $MAPbBr_3$ NP was imaged in situ underneath the ice (Fig. 2a). Then the ice was heated to room temperature in a vacuum. It is worth noting that the ice was directly vaporized without the formation of liquid water during such a heating process (as marked in Fig. S4). We performed X-ray diffraction (XRD) and photoluminescence (PL) spectra measurements before ice deposition and after ice sublimation. As shown in Fig. 2b and c, there were no detectable changes in XRD or PL spectra. Moreover, time-resolved PL (TRPL) measurements show negligible changes in carrier lifetime between original and ice-treated $MAPbBr_3$ nanoplate (Fig. S5). It indicates that neither the ice deposition nor sublimation process affects the trap-related carrier combination of perovskite crystals. We also examined the compatibility between $MAPbBr_3$ NP and solvents involved in processing conventional PMMA resists. In contrast, after immersing $MAPbBr_3$ NPs into these solvents (anisole, MIBK & IPA, IPA and acetone) for 1 min, their PL emission intensity were significantly weakened or even disappeared, and the crystals were eroded or dissolved, as demonstrated in Fig. 2d-k. These comparisons prove the superiority of iEBL on processing perovskites over conventional lithography methods. To demonstrate the general applicability of iEBL, we deposited ice resist on polycrystalline $MAPbI_3$ film. As shown in Fig. S6, the morphology of $MAPbI_3$ did not change and the grains were still densely stacked after ice sublimation. Furthermore, the PL and absorbance spectra also confirm the compatibility between $MAPbI_3$ film and ice resist.

Fig. 3a illustrates our iEBL processes for fabricating metal electrodes on $MAPbBr_3$. We chose $MAPbBr_3$ with appropriate thickness (300 nm) to prevent cracks forming during cooling it down to 130 K (Fig. S7).

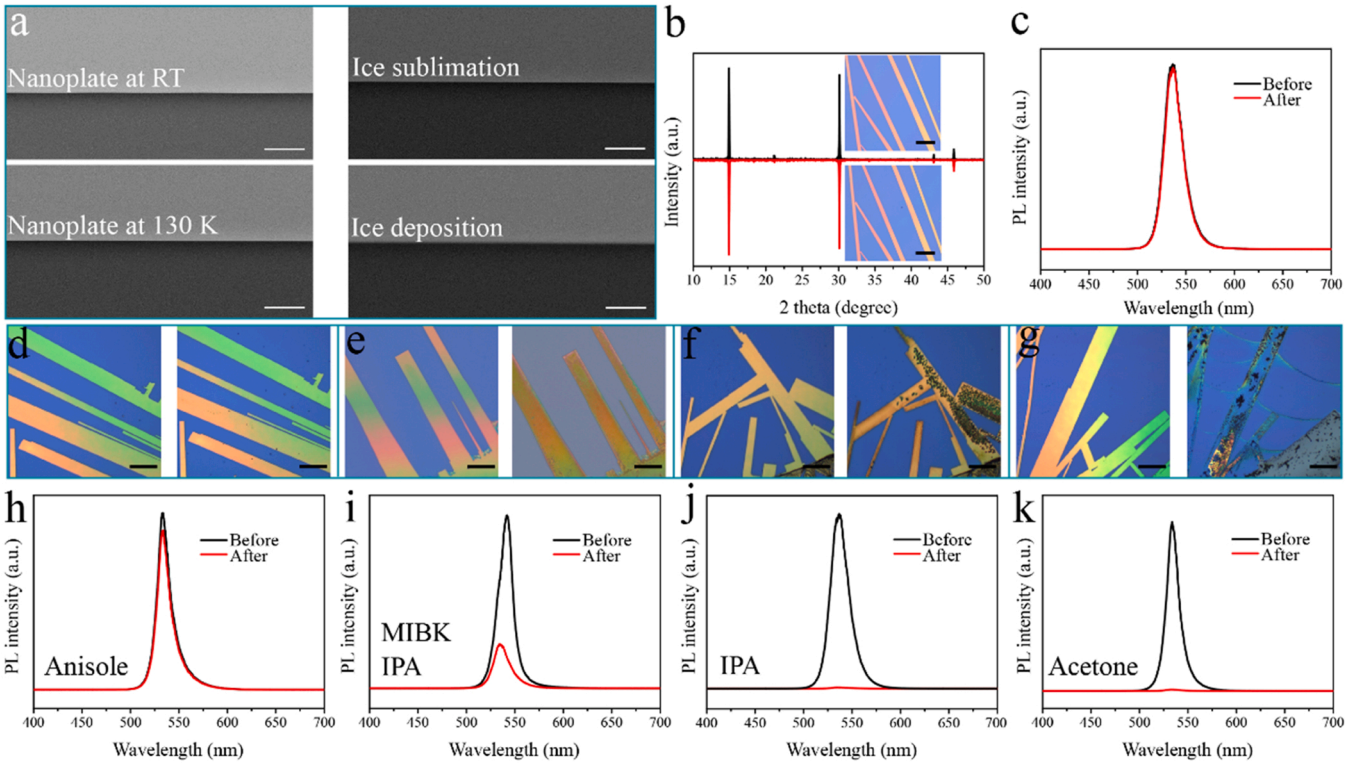

Fig. 2. Compatibility tests of $MAPbBr_3$ with ice and conventional solvents. (a) SEM images of $MAPbBr_3$ NP at room temperature and after cooling down, ice deposition and ice sublimation by rewarming to room temperature. Scale bar: 1 μm. (b) XRD and (c) PL spectra of $MAPbBr_3$ NP before ice deposition and after ice sublimation. Insets are optical images. Scale bar: 100 μm. Optical images and PL spectra of $MAPbBr_3$ NP before and after immersion in (d, h) anisole, (e, i) MIBK and IPA, (f, j) IPA and (g, k) acetone. Scale bar: 100 μm.

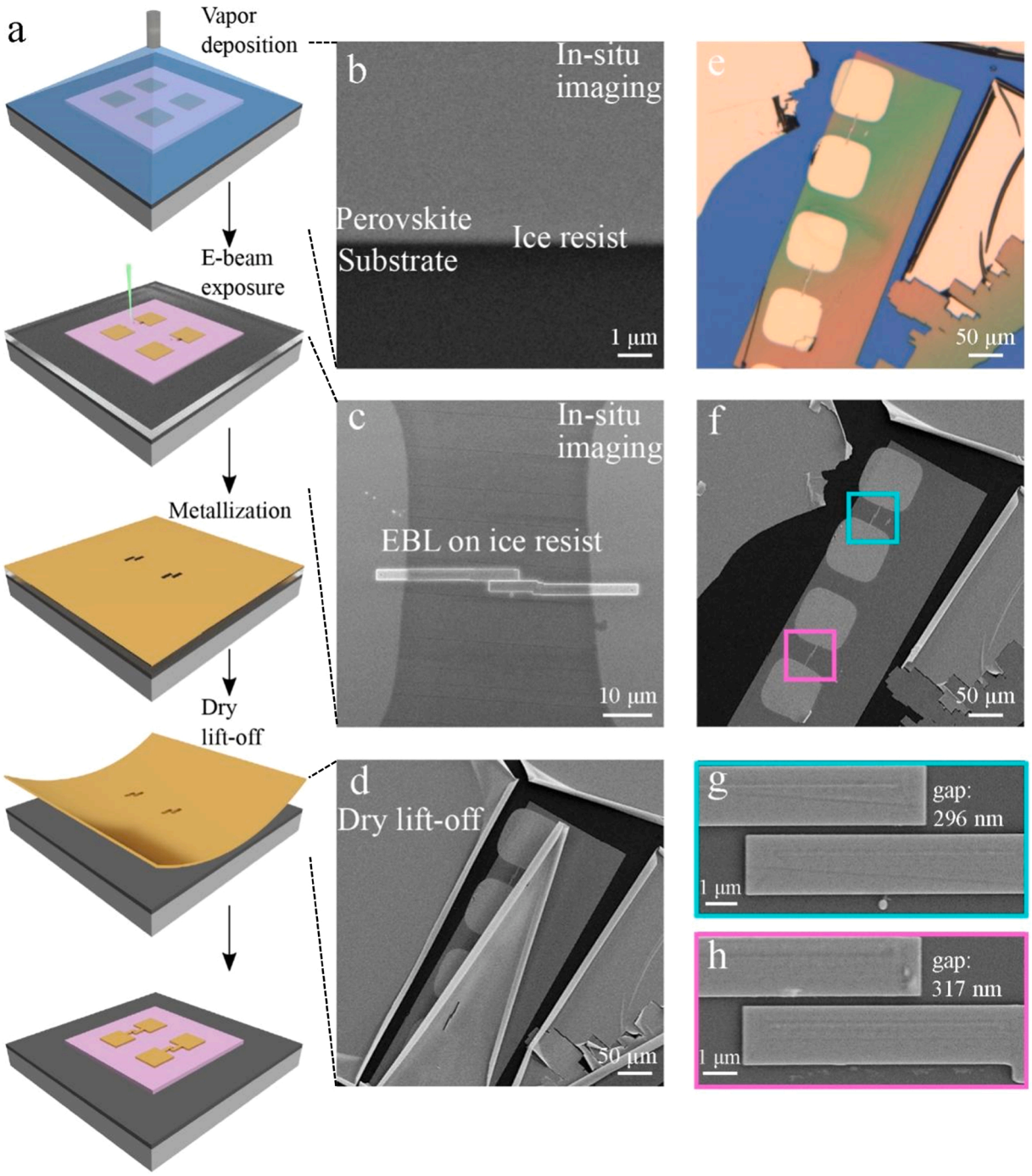

Fig. 3. IEBL fabrication process. (a) Schematic diagram for creating metal electrodes on $MAPbBr_3$ NP by iEBL. SEM images of (b) $MAPbBr_3$ NP with ice, (c) e-beam exposure on ice, (d) curly metal film before dry lift-off and (f) resultant electrodes with (g) magnified electrode gap of 296 nm and (h) 317 nm. (e) Optical image of $MAPbBr_3$ NP with electrodes.

Large-area metal pads were pre-deposited on the $MAPbBr_3$ through a shadow mask to improve the processing efficiency. Water vapor was subsequently injected onto the $MAPbBr_3$ to form a uniform film of amorphous ice with thickness of 300 nm (Fig. S8). Attributed to the advantage of in-situ imaging (Fig. 3b and c), we could directly perform e-beam exposure at desired areas and inspect the as-fabricated ice pattern immediately. Here, we employed low-energy electrons of 2 keV for patterning due to its small penetration depth of electrons as well as high yield of secondary electrons [38,39]. Dose tests were conducted (Fig. S9) in advance to determine the critical dose that just completely removed the ice without damages to the underlying perovskite. After metallization at a cryogenic temperature, the $MAPbBr_3$ was heated to room temperature to sublimate the ice. Temperature of the ice might slightly rise during the metallization process (thermal evaporation of Au). However, it did not affect the performance of the perovskite film since no liquid water formed. More SEM images for the iEBL process can be seen in Fig. S10. Finally, the residual metal film was curled and separated from the sample (Fig. 3d), which can be blown off by nitrogen gas easily. The whole iEBL process did not involve any solvents, ensuring no chemical residue and detrimental reaction with perovskite. The final electrode structure with gaps of 296 nm and 317 nm were successfully fabricated on $MAPbBr_3$ NP (Fig. 3e-h).

It is acknowledged that decreasing carrier transmission distance between the source and drain electrodes while maintaining the external quantum yield and absorption can improve the sensitivity and responsivity of a photodetector simultaneously [40,41]. In this paper, a photoconductive $MAPbBr_3$ photodetector with a small channel width of 296 nm has been obtained through the iEBL technique (Fig. 4a-b). Current-voltage (*I-V*) curves of the photodetector under dark and upon illumination (Fig. 4c and Fig. S11) imply its sensitive photoelectrical response from the ultraviolet to visible region. Fig. 4d shows good stability and fast photoresponse of the $MAPbBr_3$ photodetector after dozens of on/off switching cycles at different bias voltages of 0 V, 1 V and 3 V. When fixing the bias voltage between two electrodes at 3 V, we further obtain *I-V* curves of the photodetector under 450-nm light illumination with an irradiance varying from 12.5 to 2855 μW/cm^2 (Fig. 4e). The linear *I-V* behavior indicates good ohmic contact between the gold electrode and $MAPbBr_3$ (Fig. 4f), confirming the feasibility of iEBL technique for fabricating perovskite-based optoelectronic devices. Moreover, linearity features of the logarithmic power-photocurrent and power-responsivity curves in Fig. 4g suggest a large linear dynamic range of our $MAPbBr_3$ photodetector.

Responsivity (R_λ), detectivity (D^*) and external quantum efficiency (*EQE*) are widely used to evaluate the performance of photodetectors in terms of sensitivity, signal-to-noise ratio and photoelectric conversion efficiency of the device. They can be calculated by the following formula:

$$R_\lambda = \frac{I_{ph} - I_{dark}}{P_\lambda S}$$

$$D^* = \frac{R_\lambda}{\sqrt[2]{2eI_{dark}/S}}$$

$$EQE = \frac{hc}{e}\frac{R_\lambda}{\lambda}$$

where *e*, *h* and *c* represent the elementary charge, Plank constant and the light velocity,

considering the illumination wavelength (λ), light power density (P_λ), photocurrent (I_{ph}), dark current (I_{dark}) and effective illumination area (S) of the photodetector. Fig. 4 h and i display these three parameters of our photodetector illuminated at different light wavelengths. In fact, under the radiation intensity of 12.5 μW/cm^2 and the bias voltage of 3 V, the maximum of R_λ, D^* and *EQE* can reach 653 A/W, 3.08 × 10^{13} Jones and 180200%, respectively. Such an excellent detection performance is attributed to the formation of high-quality electrode-perovskite

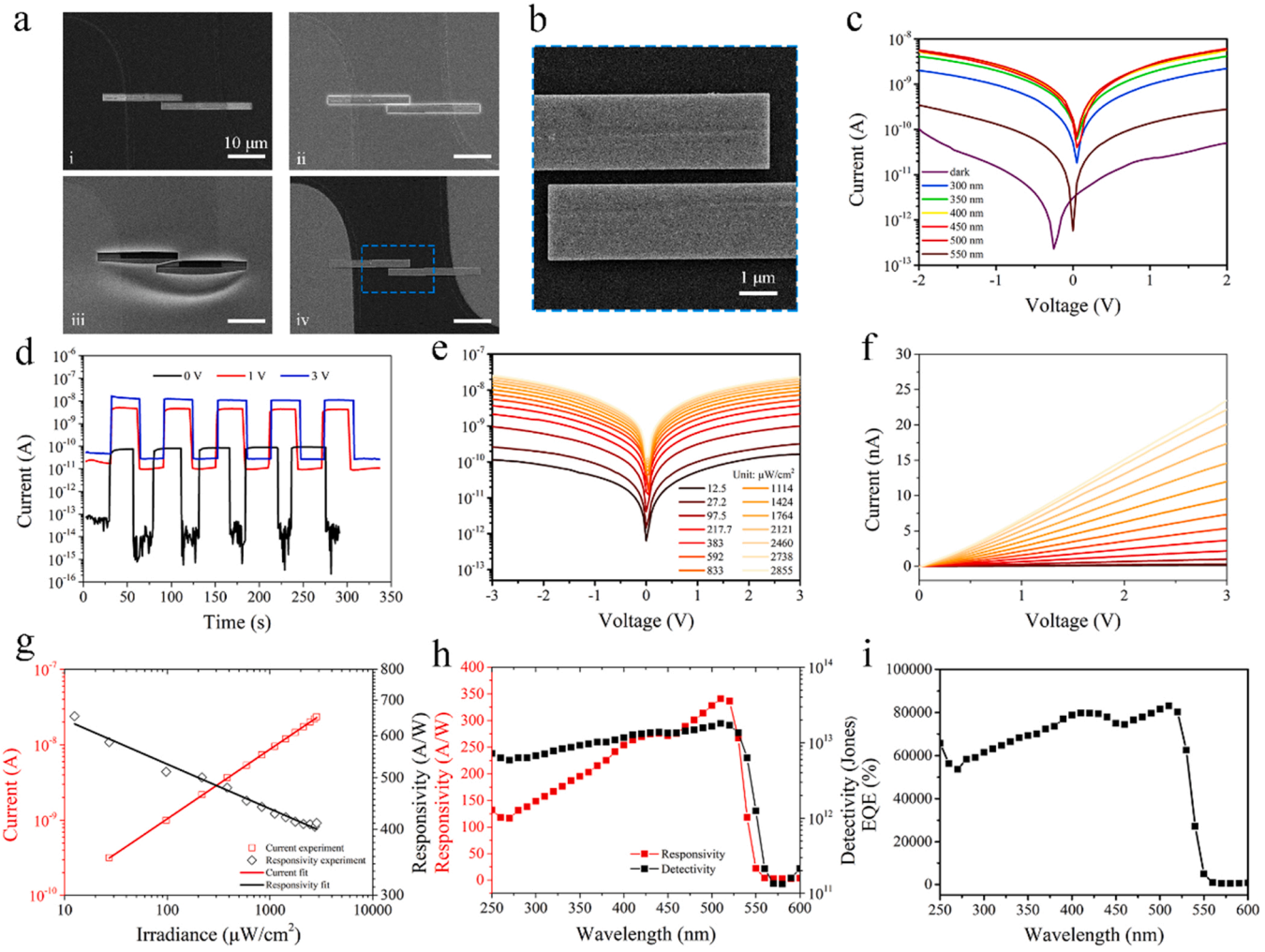

Fig. 4. Structure and characteristics of $MAPbBr_3$ photodetectors. (a) IEBL fabrication process of $MAPbBr_3$ photodetector. i: in situ e-beam exposure on ice resist; ii: metallization at 130 K; iii: residual metal films separate from the substrate after ice sublimation. iv: blown off by nitrogen gas. (b) SEM image of the $MAPbBr_3$ photodetector with a 296-nm-wide gap. (c) Semi-logarithmic *I-V* curves under dark and illumination at various light wavelengths. (d) Semi-logarithmic *I-t* curves under 450 nm illumination with on/off switching at voltage of 0, 1, and 3 V. (e) Light intensity-dependent semi-logarithmic *I–V* curves under 450 nm illumination. (f) Linear *I-V* curves of $MAPbBr_3$ photodetectors at different light irradiation. (g) Photocurrent and responsivity as a function of photodensity for $MAPbBr_3$ photodetectors. (h) Responsivity and detectivity and (i) EQE curves as a function of wavelength for $MAPbBr_3$ photodetectors.

interface and quite small electrode gap. Detailed comparisons to other $MAPbBr_3$ photodetectors fabricated through shadow mask deposition or transfer methods can be found in Table S1 in the Supplementary Information. It has been known that both responsivity and detectivity of a detector are related to illumination area. Although perovskites outside the electrode area can produce carriers under laser illumination, directional movement of carriers is quite difficult without external electric field. The responsivity and detectivity of our photodetector and those in Table S1 are estimated using the area between electrodes rather than that of the laser spot as effective illumination area.

3. Conclusion

We have demonstrated the fabrication of high-performance $MAPbBr_3$ photodetectors through developing iEBL technique. Water ice has been verified to be compatible with perovskite materials and it can be used as an effective resist for electron-beam patterning without damaging the underlying perovskite. High responsivity of 653 A/W and detectivity of more than 3×10^{13} jones have been obtained in a single $MAPbBr_3$ nanoplate device, attributed to the utterly solvent-free nanofabrication and in-situ imaging and pattering procedure in iEBL. We anticipate that the proposed iEBL process would open the door for achieving perovskite-integrated electronic and optoelectronic systems.

CRediT authorship contribution statement

Binbin Jin: Conceptualization, Methodology, Writing-Original draft preparation.**Yu Hong:** Conceptualization, Methodology. **Ziqing Li:** Methodology, Data curation, Formal analysis. **Ding Zhao:** Supervision, Visualization, Writing-Reviewing and Editing. **Yihan Lu:** Investigation. **Guangnan Yao:** Investigation. **Rui Zheng:** Investigation. **Gang Bi:** Visualization, Writing-Reviewing and Editing. **Qing Zhang:** Visualization, Writing-Reviewing and Editing. **Xiaosheng Fang:** Visualization, Resources, Writing-Reviewing and Editing. **Min Qiu:** Supervision, Project administration, Funding acquisition.

Declaration of Competing Interest

The authors declare that they have no known competing financial interests or personal relationships that could have appeared to influence the work reported in this paper.

Data availability

Data will be made available on request.

Acknowledgements

Binbin Jin, Yu Hong and Ziqing Li contributed equally to this work. The authors thank Dr. Zhong Chen and Yuan Cheng from Instrumentation and Service Center for Molecular Sciences at Westlake University for the assistance in PL measurement. The authors appreciate the supports from the National Natural Science Foundation of China (61927820, 62005226, 52072006).

Appendix A. Supporting information

Supplementary data associated with this article can be found in the online version at doi:10.1016/j.nanoen.2022.107692.

References

[1] Y. Wang, Z. Wan, Q. Qian, Y. Liu, Z. Kang, Z. Fan, P. Wang, Y. Wang, C. Li, C. Jia, et al., Probing photoelectrical transport in lead halide perovskites with van der Waals contacts, Nat. Nanotechnol. 15 (9) (2020) 768.
[2] X. Zheng, A. Calò, E. Albisetti, X. Liu, A.S.M. Alharbi, G. Arefe, X. Liu, M. Spieser, W.J. Yoo, T. Taniguchi, et al., Patterning metal contacts on monolayer MoS_2 with vanishing Schottky barriers using thermal nanolithography, Nat. Electron. 2 (1) (2019) 17.
[3] S.D. Stranks, H.J. Snaith, Metal-halide perovskites for photovoltaic and light-emitting devices, Nat. Nanotechnol. 10 (5) (2015) 391.
[4] J. Huang, Y. Yuan, Y. Shao, Y. Yan, Understanding the physical properties of hybrid perovskites for photovoltaic applications, Nat. Rev. Mater. 2 (7) (2017), 17042.
[5] D. Shi, V. Adinolfi, R. Comin, M. Yuan, E. Alarousu, A. Buin, Y. Chen, S. Hoogland, A. Rothenberger, K. Katsiev, et al., Solar cells. Low trap-state density and long carrier diffusion in organolead trihalide perovskite single crystals, Science 347 (6221) (2015) 519.
[6] W.A. Dunlap-Shohl, Y. Zhou, N.P. Padture, D.B. Mitzi, Synthetic approaches for halide perovskite thin films, Chem. Rev. 119 (5) (2019) 3193.
[7] N.J. Jeon, J.H. Noh, Y.C. Kim, W.S. Yang, S. Ryu, S.I. Seok, Solvent engineering for high-performance inorganic-organic hybrid perovskite solar cells, Nat. Mater. 13 (9) (2014) 897.
[8] W. Nie, H. Tsai, R. Asadpour, J.C. Blancon, A.J. Neukirch, G. Gupta, J.J. Crochet, M. Chhowalla, S. Tretiak, M.A. Alam, et al., Solar cells. High-efficiency solution-processed perovskite solar cells with millimeter-scale grains, Science 347 (6221) (2015) 522.
[9] Y. Peng, C. Shi, Y. Zhu, M. Gu, S. Zhuang, Terahertz spectroscopy in biomedical field: a review on signal-to-noise ratio improvement, PhotoniX 1 (2020), 12.
[10] N. Zhang, W. Sun, S.P. Rodrigues, K. Wang, Z. Gu, S. Wang, W. Cai, S. Xiao, Q. Song, Highly reproducible organometallic halide perovskite microdevices based on top-down lithography, Adv. Mater. 29 (15) (2017) 1606250.
[11] L. Gao, K. Zeng, J. Guo, C. Ge, J. Du, Y. Zhao, C. Chen, H. Deng, Y. He, H. Song, et al., Passivated single-crystalline $CH_3NH_3PbI_3$ nanowire photodetector with high detectivity and polarization sensitivity, Nano Lett. 16 (12) (2016) 7446.
[12] R. Xiao, Y. Hou, Y. Fu, X. Peng, Q. Wang, E. Gonzalez, S. Jin, D. Yu, Photocurrent mapping in single-crystal methylammonium lead iodide perovskite nanostructures, Nano Lett. 16 (12) (2016) 7710.
[13] E. Ozbay, Plasmonics: merging photonics and electronics at nanoscale dimensions, Science 311 (5758) (2006) 189.
[14] E. Menard, M.A. Meitl, Y. Sun, J.U. Park, D.J. Shir, Y.S. Nam, S. Jeon, J.A. Rogers, Micro- and nanopatterning techniques for organic electronic and optoelectronic systems, Chem. Rev. 107 (4) (2007) 1117.
[15] Y. Liu, Y. Zhang, K. Zhao, Z. Yang, J. Feng, X. Zhang, K. Wang, L. Meng, H. Ye, M. Liu, et al., A 1300 mm^2 ultrahigh-performance digital imaging assembly using high-quality perovskite single crystals, Adv. Mater. 30 (29) (2018) 1707314.
[16] Y. Liu, Y. Zhang, Z. Yang, J. Feng, Z. Xu, Q. Li, M. Hu, H. Ye, X. Zhang, M. Liu, et al., Low-temperature-gradient crystallization for multi-inch high-quality perovskite single crystals for record performance photodetectors, Mater. Today 22 (2019) 67.
[17] R. Ding, C.K. Liu, Z. Wu, F. Guo, S.Y. Pang, L.W. Wong, W.F. Io, S. Yuan, M. C. Wong, M.B. Jedrzejczyk, et al., A general wet transferring approach for diffusion-facilitated space-confined grown perovskite single-crystalline optoelectronic thin films, Nano Lett. 20 (4) (2020) 2747.
[18] H. Jing, R. Peng, R.M. Ma, J. He, Y. Zhou, Z. Yang, C.Y. Li, Y. Liu, X. Guo, Y. Zhu, et al., Flexible Ultrathin Single-Crystalline Perovskite Photodetector, Nano Lett. 20 (10) (2020) 7144.
[19] Y. Bai, H. Zhang, M. Zhang, D. Wang, H. Zeng, J. Zhao, H. Xue, G. Wu, J. Su, Y. Xie, et al., Liquid-phase growth and optoelectronic properties of two-dimensional hybrid perovskites $CH_3NH_3PbX_3$ (X = Cl, Br, I), Nanoscale 12 (2) (2020) 1100.
[20] Z. Gu, Z. Huang, C. Li, M. Li, Y. Song, A general printing approach for scalable growth of perovskite single-crystal films, Sci. Adv. 4 (6) (2018) eaat2390.
[21] C.H. Lin, B. Cheng, T.Y. Li, J.R.D. Retamal, T.C. Wei, H.C. Fu, X. Fang, J.H. He, Orthogonal lithography for halide perovskite optoelectronic nanodevices, ACS Nano 13 (2) (2019) 1168.
[22] A. Daus, C. Roldan-Carmona, K. Domanski, S. Knobelspies, G. Cantarella, C. Vogt, M. Gratzel, M.K. Nazeeruddin, G. Troster, Metal-halide perovskites for gate dielectrics in field-effect transistors and photodetectors enabled by PMMA lift-off process, Adv. Mater. 30 (23) (2018), 1707412.
[23] Y. Hong, D. Zhao, D. Liu, B. Ma, G. Yao, Q. Li, A. Han, M. Qiu, Three-dimensional in situ electron-beam lithography using water ice, Nano Lett. 18 (8) (2018) 5036.
[24] Y. Hong, D. Zhao, J. Wang, J. Lu, G. Yao, D. Liu, H. Luo, Q. Li, M. Qiu, Solvent-free nanofabrication based on ice-assisted electron-beam lithography, Nano Lett. 20 (12) (2020) 8841.
[25] H.S. Rao, W.G. Li, B.X. Chen, D.B. Kuang, C.Y. Su, In situ growth of 120 cm^2 $CH_3NH_3PbBr_3$ perovskite crystal film on FTO glass for narrowband-photodetectors, Adv. Mater. 29 (16) (2017) 1602639.
[26] Z. Yang, Y. Deng, X. Zhang, S. Wang, H. Chen, S. Yang, J. Khurgin, N.X. Fang, X. Zhang, R. Ma, High-performance single-crystalline perovskite thin-film photodetector, Adv. Mater. 30 (8) (2018), 1704333.
[27] Y.X. Chen, Q.Q. Ge, Y. Shi, J. Liu, D.J. Xue, J.Y. Ma, J. Ding, H.J. Yan, J.S. Hu, L. J. Wan, General Space-Confined On-Substrate Fabrication of Thickness-Adjustable Hybrid Perovskite Single-Crystalline Thin Films, J. Am. Chem. Soc. 138 (50) (2016) 16196.
[28] Z. Chen, Q. Dong, Y. Liu, C. Bao, Y. Fang, Y. Lin, S. Tang, Q. Wang, X. Xiao, Y. Bai, et al., Thin single crystal perovskite solar cells to harvest below-bandgap light absorption, Nat. Commun. 8 (1) (2017) 1890.
[29] W. Yu, F. Li, L. Yu, M.R. Niazi, Y. Zou, D. Corzo, A. Basu, C. Ma, S. Dey, M.L. Tietze, et al., Single crystal hybrid perovskite field-effect transistors, Nat. Commun. 9 (1) (2018) 5354.
[30] Y. Liu, Y. Zhang, Z. Yang, D. Yang, X. Ren, L. Pang, S.F. Liu, Thinness- and shape-controlled growth for ultrathin single-crystalline perovskite wafers for mass production of superior photoelectronic devices, Adv. Mater. 28 (41) (2016) 9204.

[31] Y. Liu, Y. Zhang, Z. Yang, H. Ye, J. Feng, Z. Xu, X. Zhang, R. Munir, J. Liu, P. Zuo, et al., Multi-inch single-crystalline perovskite membrane for high-detectivity flexible photosensors, Nat. Commun. 9 (1) (2018) 5302.
[32] X.D. Wang, W.G. Li, J.F. Liao, D.B. Kuang, Recent advances in halide perovskite single-crystal thin films: fabrication methods and optoelectronic applications, Sol. RRL 3 (4) (2019), 1800294.
[33] J.A. Christians, P.A. Miranda Herrera, P.V. Kamat, Transformation of the excited state and photovoltaic efficiency of $CH_3NH_3PbI_3$ perovskite upon controlled exposure to humidified air, J. Am. Chem. Soc. 137 (4) (2015) 1530.
[34] A.M.A. Leguy, Y. Hu, M. Campoy-Quiles, M.I. Alonso, O.J. Weber, P. Azarhoosh, M. van Schilfgaarde, M.T. Weller, T. Bein, J. Nelson, et al., Reversible hydration of $CH_3NH_3PbI_3$ in films, single crystals, and solar cells, Chem. Mater. 27 (9) (2015) 3397.
[35] C. Müller, T. Glaser, M. Plogmeyer, M. Sendner, S. Döring, A.A. Bakulin, C. Brzuska, R. Scheer, M.S. Pshenichnikov, W. Kowalsky, et al., Water infiltration in methylammonium lead iodide perovskite: fast and inconspicuous, Chem. Mater. 27 (22) (2015) 7835.
[36] G.E. Eperon, S.N. Habisreutinger, T. Leijtens, B.J. Bruijnaers, J.J. van Franeker, D. W. deQuilettes, S. Pathak, R.J. Sutton, G. Grancini, D.S. Ginger, et al., The Importance of Moisture in Hybrid Lead Halide Perovskite Thin Film Fabrication, ACS Nano 9 (9) (2015) 9380.
[37] W. Zhou, Y. Zhao, C. Shi, H. Huang, J. Wei, R. Fu, K. Liu, D. Yu, Q. Zhao, Reversible healing effect of water molecules on fully crystallized metal–halide perovskite film, J. Phys. Chem. C 120 (9) (2016) 4759.
[38] M.U. Rothmann, W. Li, Y. Zhu, A. Liu, Z. Ku, U. Bach, J. Etheridge, Y.B. Cheng, Structural and chemical changes to $CH_3NH_3PbI_3$ induced by electron and gallium ion beams, Adv. Mater. 30 (25) (2018), 1800629.
[39] N. Yi, S. Wang, Z. Duan, K. Wang, Q. Song, S. Xiao, Tailoring the performances of lead halide perovskite devices with electron-beam irradiation, Adv. Mater. 29 (34) (2017), 1701636.
[40] B. Peng, H. Zhou, Z. Liu, Y. Li, Q. Shang, J. Xie, L. Deng, Q. Zhang, D. Liang, Pattern-selective molecular epitaxial growth of single-crystalline perovskite arrays toward ultrasensitive and ultrafast photodetector, Nano Lett. 22 (7) (2022) 2948–2955.
[41] W. Wen, W. Zhang, X. Wang, Q. Feng, Z. Liu, T. Yu, Ultrasensitive photodetectors promoted by interfacial charge transfer from layered perovskites to chemical vapor deposition-grown MoS_2, Small 17 (36) (2021), 2102461.

Binbin Jin received his Ph.D. degrees from Technical Institute of Physics and Chemistry, Chinese Academy of Sciences in 2019. He then worked as a postdoctoral fellow in the school of engineering at Westlake University during 2019–2021. In 2022, he became a research assistant at Zhejiang University City College. Currently, his research focuses on micro-nano fabrication based on the technology of ice lithography.

Ziqing Li received his B.S. and Ph.D. degrees from Shandong University in 2014 and 2019. He worked as a postdoctoral fellow in the Department of Materials Science at Fudan University during 2019–2021. In 2022, he became a research associate at Fudan University. Currently, his research focuses on optoelectronic devices based on solution-processed perovskites and inorganic semiconductors.

Yu Hong received his Ph.D. degree in optical engineering from Zhejiang University in 2021. His research focuses on ice-assisted electron beam lithography for nanofabrication and its applications in nanophotonis, etc.

Ding Zhao received his Ph.D. degree in Optical Engineering from Zhejiang University, China in 2016. From 2016–2019, he worked as a postdoctoral researcher at Zhejiang University and a H.C. Ørsted postdoctoral fellow at Technical University of Denmark. He became a research assistant professor and research associate professor in 2020 and 2022, respectively. His research interests focus on advanced nanolithography and nanopatterning methods.

Yihan Lu is currently pursuing her Ph.D. degree in Engineering School, Westlake University, China. Her research mainly focuses on ice lithography and micro/nano device fabrication.

Guangnan Yao is currently pursuing the Ph.D. degree in Institute of Optical Engineering, Zhejiang University, Zhejiang, China. His research focuses on nanofabrication using ice-assisted electron beam lithography and 2D materials devices.

Rui Zheng got his Bachelor degree in Zhejiang University in 2020. Currently, he is pursuing the Ph.D. degree in Electronic Science and Technology from Westlake University, Hangzhou, China. His research interests focus on nanofabrication technology and nanophotonics.

Gang Bi is currently a professor in school of information & electrical engineering at Zhejiang University City College. He received Ph.D. degree from Zhejiang University in 2000. He was a visiting scholar at University of Oklahoma and UC Berkeley in 2008 and 2015, respectively. His current research topic mainly focuses on surface plasmons and photoelectric materials and devices.

Qing Zhang received Ph.D. degree from Tsinghua University in 2011. She then engaged in post-doctoral research at Nanyang Technological University from 2011 to 2016. Since 2016, she served as a professor in school of materials science and engineering, Peking University. Her research interests include nanophotonics, surface plasmons and low-dimensional semiconductor materials and devices.

Xiaosheng Fang is currently a professor in Department of Materials Science at Fudan University, China. He received his Ph.D. degree from the Institute of Solid State Physics (ISSP), Chinese Academy of Sciences in 2006. After then, he was JSPS postdoctoral fellow and research scientist at the National Institute for Materials Science (NIMS), Japan. He was a visiting scholar at MIT and Harvard University in 2009 and 2016, respectively. His current research topic mainly focuses on inorganic semiconductors and optoelectronic applications.

Min Qiu received his Ph.D. degree in Physics from Zhejiang University, China in 1999. He became an assistant professor and a full professor at the Royal Institute of Technology (KTH), Sweden, in 2001 and 2009, respectively. Since 2010, he worked as a professor at Zhejiang University. He was the director of State Key Laboratory of Modern Optical Instrumentation, Zhejiang University. In 2018 he joined Westlake University as a Guoqiang chair professor and vice president for research. His research interests include nanofabrication technology, nanophotonics, and green photonics.